Palaeogeography, Palaeoclimatology, Palaeoecology 293 (2010) 144–156

Contents lists available at ScienceDirect

Palaeogeography, Palaeoclimatology, Palaeoecology

journal homepage: www.elsevier.com/locate/palaeo

Environmental magnetic study of a Xeralf chronosequence in northwestern Spain: Indications for pedogenesis

Qingsong Liu [a,*], Pengxiang Hu [a], José Torrent [b], Vidal Barrón [b], Xiangyu Zhao [a], Zhaoxia Jiang [a], Youliang Su [a,c]

[a] State Key Laboratory of Lithospheric Evolution (SKL-LE), Institute of Geology and Geophysics, Chinese Academy of Sciences, Beijing 100029, China
[b] Departamento de Ciencias y Recursos Agrícolas y Forestales, Universidad de Córdoba, Edificio C4, Campus de Rabanales, 14071 Córdoba, Spain
[c] Institute of Tibetan Plateau Research, Chinese Academy of Sciences, Beijing 100085, China

ARTICLE INFO

Article history:
Received 16 February 2010
Received in revised form 13 May 2010
Accepted 19 May 2010
Available online 26 May 2010

Keywords:
Soil magnetism
Chronosequence
Pedogenesis

ABSTRACT

Magnetic enhancement of A and B horizons during soil development is a common phenomenon. To better understand the exact mechanism for the magnetic enhancement, especially the mineral transformation pathways, systematic rock magnetic studies were conducted on a Xeralf chronosequence in northwestern Spain. A positive correlation was found between the average grain size and the concentration of pedogenic maghemite particles with the exception of some A horizons, in which multiple factors seem to influence the nature and concentration of neoformed ferrimagnets. It is argued that the interaction between the positively charged iron oxides and the anionic ligands present in the solution of these acidic soils plays an important role in this respect. The time trends of the average grain size of pedogenic ferrimagnets and the strong correlation between the concentrations of hematite and maghemite in the magnetically enhanced horizons (A and B) are consistent with the hypothesis of a gradual formation of maghemite (later converted into hematite) via a precursor (most likely ferrihydrite). Therefore, this study provides strong evidence for the dynamic evolution of magnetic minerals upon pedogenesis.

1. Introduction

Soil formation (pedogenesis) involves a series of changes in the chemical and physical properties of the parent material in any given environment (Vincent et al., 1994). Specifically, the mineral assemblage (including magnetic minerals) in soils changes with time under the integrated effects of the soil forming factors (parent material, climate, organisms, and relief) (Jenny, 1941, 1980). Among the pedogenic minerals, the magnetic ones play an important role in diagnosing the dynamics of pedogenic processes (Zhou et al., 1990; Singer et al., 1996; Liu et al., 2005a,b), thereby improving our understanding of the linkage between magnetic properties and climatic conditions (Maher et al., 1994; Deng et al., 2005, 2006).

Due to the downward propagation processes involved, soils consist typically of several interrelated horizons: the A horizon, a layer which is characterized by the accumulation of organic matter and, usually, loss of some soluble and/or mobile components (such as silicate clays, iron, aluminum and humic substances); the B horizon, a layer characterized by significant alteration of the parent material or by accumulation of the constituents leached from the overlying A horizon; and the C horizon, the relatively unaltered parent material. Most often, the magnetic properties are enhanced in the A and B horizons due to weathering of Fe-bearing minerals and the subsequent neoformation of nanosized ferrimagnets (magnetite and/or maghemite) (Zhou et al., 1990; Maher, 1998; Liu et al., 2005b). Previous studies on modern soils showed that, unless Fe was leached from the soil (following reductive dissolution of the Fe oxides or complexation of Fe with humic substances), the concentration of these minerals was positively correlated to the annual precipitation (Heller et al., 1993; Maher et al., 1994; Han et al., 1996; Liu et al., 2005a). Such observations, which are implicitly based on the close relationship between degree of weathering and precipitation, have been further extended to past geological periods to construct the possible evolution of paleoprecipitation (Maher et al., 1994).

Parallel to their ferrimagnetic counterparts, antiferromagnetic minerals (e.g. hematite, goethite) are also formed in the course of pedogenesis (Verosub et al., 1993; Liu et al., 2003; Chen et al., 2005). In this context, the ratio of maghemite to hematite has been suggested to be a paleorainfall proxy superior to the magnetic susceptibility (Liu et al., 2007a; Torrent et al., 2006, 2010a,b). In addition, the grain size distribution of pedogenic ferrimagnets bears significant information concerning the pedogenic environment (Liu et al., 2005b; Torrent et al., 2010a). Therefore, to determine the exact pathways of pedogenic processes, it is necessary to fully interpret the significance of the nature and properties of magnetic minerals in soils and their relationships with other iron oxides.

* Corresponding author.
E-mail address: qsliu@mail.iggcas.ac.cn (Q. Liu).

0031-0182/$ – see front matter © 2010 Elsevier B.V. All rights reserved.
doi:10.1016/j.palaeo.2010.05.008

To elucidate how pedogenic processes affect the formation and preservation of magnetic minerals, modern soils (Maher et al., 2002; Blundell et al., 2009), loess–paleosol sequences (Heller and Liu, 1986; Kukla et al., 1988; Verosub et al., 1993; Evans and Heller, 1994; Liu et al., 2007a), and soil chronosequences (e.g. Singer et al., 1992) have been investigated. Compared to modern soils, the soils in pristine chronosequences were formed under similar conditions of parent material, climate, vegetation, and relief, time being the only variable (Jenny, 1941; Bockheim, 1980; Birkeland, 1984; Kelly and Yonker, 2005). This allows us to investigate the time-related issues, e.g. the rate and direction of pedogenic changes. Unlike the loess–paleosol sequences, where the pedogenic processes were terminated once the soil was buried, soils in chronosequences can be in a dynamic equilibrium with the environment (Huggett, 1998).

In this study, we investigate the soils in a chronosequence of river terraces in north-western Spain. Systematic studies on the subtle changes in magnetic properties and the relationships between the different iron oxides for this sequence can provide invaluable information for better understanding of how pedogenesis functions.

2. Geological setting, soil sampling, and measurements

The soil chronosequence is located in the central part of the Esla River valley, Castilla la Vieja Plateau, north-western Spain (41° 02–28′ N, 5° 14–51′ W; average altitude: 800 m), and described in detail by Torrent (1975, 1976) and Torrent et al. (2010b). The present climate is continental Mediterranean with mean annual temperature of 11.5 °C (3 °C in January and 20 °C in July) and mean annual precipitation of 550 mm with only 100 mm falling in summer. The sequence comprises 13 terrace levels ranging in altitude from 3 to 160 m above the present river level (Table 1) (Torrent et al., 2010b). Except for the terrace at 3 m (with an age of ~3.3 kyr (Torrent, 1976)), no precise dating of the other terraces is available, although the highest one is probably >1 Myr old (A. Martín-Serrano, personal communication). The terrace deposits are 2–10 m thick and their materials sources were Paleozoic rocks. The parent alluvium is generally rich in stones and gravel of quartzite and the fine earth (<2 mm) fraction ranges widely in grain size distribution. Quartz is the dominant mineral in the non-clay fraction, and illite and interstratified illite/vermiculite are dominant in the clay (<2 μm) fraction. In the fresh alluvium, this fraction contains 5–10% of goethite but only traces of hematite. Therefore, the hematite in the magnetically enriched layers can be confidently attributed to pedogenesis.

The soils are Typic or Ultic Haplo- or Palexeralfs according to Soil Taxonomy (Soil Survey Staff, 2006). Micromorphological observations indicated that substantial translocation of clay from the A to the B horizons took place during pedogenesis, so the proportion of clay in the fine earth is 90–190 g kg^{-1} in the present ploughed topsoil (Ap horizon) and 140–820 g kg^{-1} in the horizon with translocated clay (i.e. the Bt horizon). The Bt horizon generally comprises several subhorizons (named Bt1, Bt2, etc.) and, except for the two youngest soils, extends to a depth of >150 cm. The degree of rubification (reddening) increases with increasing soil age because of the increase in the proportion of pedogenic hematite up to the 48-m terrace. The downward propagation of the pedogenic process results in a gradual change in magnetic properties from A to B horizons (Fig. 1).

Above the 48 m level, the soils contain little or no hematite in their Bt horizons. This is due to the existence of a perched water table in the winter months resulting in reductive dissolution of this mineral and maghemite while leaving relatively unaltered the accompanying Al-substituted goethite, as usually observed in many redoximorphic soils (Barrón and Torrent, 1987). This perched water table, which is evident from seepage areas in lower landscape positions, is thought to arise as a result of the reduction in hydraulic conductivity resulting from the accumulation of translocated clay in the pores of the Bt horizons. Its upper limit reaches almost the soil surface in some years in the soils on the terraces above the 95 m level; its lower limit, which is marked by an increase in the proportion of areas with red hues, is at a depth of 160–80 cm.

The soils were originally described and sampled in the summer of 1973 (Torrent, 1976). Samples were taken from the Ap horizon and the 3–4 subhorizons of the Bt (argillic) horizon (Bt proper in the case of moderately well drained subhorizons and Btg in the case of subhorizons undergoing seasonal reduction due to the presence of the perched water table). The samples were dried, ground, sieved (<2 mm), and kept in polyethylene bags in a dry (relative humidity<55%) storage area for further use.

The basic properties of the soils and the corresponding standard analytical methods were reported in detail by Torrent (1975, 1976). For various mineralogical and magnetic studies used only the clay fraction, which was previously separated by sedimentation (Torrent et al., 2010b). The reason was that the non-clay fraction did not contain significant amounts of pedogenic Fe oxides (including the ferrimagnets) (Torrent et al., 2010b). Details of the diffuse reflectance spectroscopy (DRS) method to estimate the absolute mass concentrations of hematite (Hm) and goethite (Gt) can be found by Torrent et al. (2007). Basically, the DR spectra were recorded from 380 to 710 nm in 0.5 nm steps. The measured reflectance values were then transformed into the Kukelka–Munk remission function. The second derivative of this function in the 380–710 nm range was calculated using a cubic spline procedure and the ratio of intensities of the bands around 425 (for goethite) and 535 nm (for hematite) were used to estimate the relative concentrations of goethite and hematite; the coefficient of variation of this procedure is 10–15%. The absolute concentrations of goethite and hematite were calculated by assigning the citrate/bicarbonate/dithionite (CBD)-extractable Fe (Fe_d) to these two minerals because this extractant is considered to be selective for the Fe oxides (Mehra and Jackson, 1958), and the mass contribution from maghemite, which is also CBD-soluble, to Fe_d is rather limited (Torrent et al., 2007).

The magnetic susceptibility (χ, mass-specific) was measured using a Bartington MS-2 magnetic susceptibility meter at dual frequencies of 470 Hz (low frequency) and 4700 Hz (high frequency). The corresponding χ values are referred to χ_{LF} and χ_{HF}, respectively. To detect the presence of the magnetically viscous fine-grained ferrimagnetic particles (those located near the boundary between the single domain, SD, and superparamagnetic, SP, regions; Worm, 1998), the absolute frequency-dependent susceptibility, $\chi_{fd} = (\chi_{LF} - \chi_{HF})$, and the percent frequency-dependent susceptibility, $\chi_{fd}\% = ((\chi_{fd}/\chi_{LF}) \times 100)$ were calculated. Generally, χ_{fd} is proportional to the concentration and χ_{fd}% is inversely related to the width of the grain size distribution of these viscous SP particles (Worm, 1998).

Low-temperature-dependence χ curves were measured between 5 K and 300 K using a Quantum Designs Magnetic Properties Measurement System (MPMS). The working frequencies were set to be 1 and 10 Hz, respectively; note in this respect that, for the low-temperature measurements, χ_{fd} is defined as $\chi_{1\,Hz} - \chi_{10\,Hz}$. The applied field was set to be 0.4 mT. Because of the noisy pattern for the weakly magnetic samples, to estimate the temperature ($T_{\chi fd\text{-}max}$) for the maximum χ_{fd} value, the χ_{fd}–T curves were fitted to a polynomial curve. The root mean square deviation was calculated to evaluate the 'goodness of fit' (Liu et al., 2004a). Overall, a 3rd-order polynomial successfully fits the curve, and is consistently applied to all curves. For several samples with $T_{\chi fd\text{-}max}$ slightly >300 K, the fitted polynomial curve was extrapolated up to 400 K to estimate the corresponding $T_{\chi fd\text{-}max}$.

Anhysteretic remanent magnetization (ARM) was measured in an alternating field (AF) of 150 mT with a superimposed 50 μT bias field. The concentrations of hematite and/or goethite in the samples are related to "hard" isothermal remanent magnetization (HIRM), which is defined as $0.5 \times (SIRM + IRM_{-300\,mT})$, where SIRM and $IRM_{-300\,mT}$ represent the

Table 1
Summary of both magnetic and non-magnetic proxies for the Esla soil chronosequence.

Name	Depth (cm)	χ	χ_{fd}	$\chi_{fd\%}$	SIRM	χ_{arm}	S-300	HIRM	L	Fe_d	Hm	Gt	Hm/(Hm + Gt)	Gt/(Hm + Gt)	M_s	M_{rs}/M_s	B_c	B_{cr}	B_{cr}/B_c	χ/M_s	$T_{\chi fd,max}$
3-M A_P	0–23	21.1	2.3	10.9	1.167	1.37E−05	0.94	7.3	0.57	53.8	7	69	0.09	0.91							250
3-M Bt1	23–64	11	1.4	12.7	0.443	4.56E−06	0.85	6.7	0.66	62.7	8	82	0.09	0.91	3.4	0.16	4.32	19.64	4.55	3.3	245
3-M Bt2	64–90	15.3	1.8	11.8	0.598	5.79E−06	0.89	6.6	0.63	65.7	9	86	0.1	0.91	4.4	0.18	4.43	16.86	3.81	3.5	245
3-M Bt3	90–140	15.4	1.9	12.3	0.484	5.06E−06	0.88	5.9	0.66	65.9	9	87	0.09	0.91							240
3-M C	140–160	15.2	2	13.2	0.434	4.69E−06	0.86	6.1	0.68	69.6	9	93	0.09	0.91	4.2	0.16	3.12	16.05	5.14	3.6	250
8-M A_P	0–20	44.3	4.9	11.1	2.472	2.54E−05	0.95	12.8	0.57	56.9	24	53	0.31	0.69	16.6	0.18	5.42	19.43	3.58	2.7	335
8-M Bt1	20–53	45.5	5.1	11.2	1.877	1.99E−05	0.94	11.1	0.63	62.1	28	59	0.32	0.68	19.1	0.15	4.56	17.83	3.91	2.4	310
8-M Bt2	53–102	12.8	1.8	14.1	0.470	5.02E−06	0.84	7.4	0.69	71.8	15	91	0.15	0.86	4.7	0.15	4.29	21.73	5.07	2.8	290
8-M Bt3	102–130	11.1	1.5	13.5	0.377	4.35E−06	0.83	6.5	0.67	66.1	14	84	0.14	0.86	3.1	0.13	3.94	23.6	5.99	3.5	270
8-M C	130–170	10.9	1.5	13.8	0.356	3.93E−06	0.82	6.3	0.66	63.3	12	81	0.13	0.87	3.4	0.15	3.92	21.82	5.57	3.2	270
11-M A_P	0–22	63.4	7.3	11.5	3.126	3.09E−05	0.96	11.3	0.49	60.8	29	53	0.35	0.65	25.3	0.15	5.03	18.43	3.66	2.5	245
11-M Bt1	22–50	26.8	3.3	12.3	1.063	1.13E−05	0.90	11.0	0.59	67.8	23	72	0.24	0.76	7.8	0.15	4.19	18.65	4.45	3.4	240
11-M Bt2	50–85	13.4	1.7	12.7	0.425	3.81E−06	0.78	9.2	0.66	68.9	17	83	0.17	0.83	4.1	0.15	3.89	24.1	6.20	3.3	235
11-M Bt3	85–135	8.5	1.1	12.9	0.259	2.04E−06	0.73	6.9	0.70	63.5	12	80	0.13	0.87							245
11-M Bt4	135–172	8.8	1.2	13.6	0.247	2.06E−06	0.74	6.4	0.69	65	13	82	0.14	0.86							270
20-M Bt1	21–60	20.2	2.6	12.9	0.580	5.84E−06	0.91	5.5	0.64	67.9	41	59	0.41	0.59	4.9	0.14	3.28	17.23	5.25	4.1	
20-M Bt2	60–98	12.1	1.7	14.0	0.273	3.08E−06	0.84	4.4	0.68	59.2	27	61	0.3	0.69	2.7	0.13	3.06	23.31	7.62	4.5	
20-M Bt3	98–155	7.6	0.9	11.8	0.204	1.98E−06	0.77	4.7	0.69	61.3	13	80	0.14	0.86	1.8	0.16	2.82	19.58	6.94	4.1	
45-M A_P	0–27	84.5	9.2	10.9	4.298	4.18E−05	0.97	13.8	0.49	71.6	38	61	0.38	0.62	33.4	0.16	5.07	1.87E+01	3.69	2.5	345
45-M Bt1	27–68	45.5	6.1	13.4	1.469	1.73E−05	0.94	8.9	0.58	74.2	45	61	0.42	0.58	12.5	0.13	3.89	17.96	4.62	3.6	300
45-M Bt2	68–112	26.7	3.8	14.2	0.788	1.00E−05	0.89	8.5	0.73	82.1	44	74	0.37	0.63	6.6	0.13	3.38	17.66	5.22	4.0	275
45-M Bt3	112–157	7.7	1	13.0	0.186	1.51E−06	0.66	6.3	0.74	95	23	121	0.16	0.84	1.4	0.13	3.05	24.96	8.18	5.7	245
48-M A_P	0–20	59.6	7.7	12.9	2.219	2.91E−05	0.95	10.1	0.56	69.2	41	55	0.42	0.57	15.7	0.15	3.95	18.13	4.59	3.8	220
48-M Bt1	20–60	18.7	2.5	13.4	0.487	6.49E−06	0.89	5.5	0.65	70.4	33	70	0.32	0.68	4.4	0.14	3.5	18.1	5.17	4.3	270
48-M Bt2	60–100	5.4	0.7	13.0	0.129	1.24E−06	0.72	3.6	0.69	66.5	12	90	0.11	0.88	1.2	0.13	3.42	2.43E+01	7.11	4.4	220
48-M Bt3	100–135	2.4	0.2	8.3	0.080	3.59E−07	0.52	3.8	0.72	71	10	98	0.1	0.91							230
77-M A_P	0–22	19.2	2.4	12.5	0.832	1.06E−05	0.94	5.2	0.58	74.3	12	93	0.12	0.89	7.9	0.18	4.54	17.65	3.89	2.4	305
77-M Bt1	22–54	5.1	0.6	11.8	0.146	1.39E−06	0.77	3.4	0.72	63.4	8	87	0.09	0.92	1.3	0.15	3.8	24.01	6.32	4.1	
77-M Bt2	54–122	1.2	0	0.0	0.050	7.75E−08	0.68	1.6	0.85	54.5	0	85	0	1.00	0.2	0.24	17.29			6.9	
77-M Btg	122–155	1.3	0	0.0	0.043	1.02E−07	0.44	2.4	0.81	51	0	79	0	1.00	0.4	0.17	16.87			3.0	
85-M A_P	0–25	15.3	1.9	12.4	0.803	9.71E−06	0.92	6.1	0.63	81.8	9	106	0.08	0.92	5.9	0.18	5.15	19.7	3.83	2.6	275
85-M Bt1	25–47	3.7	0.4	10.8	0.117	9.07E−07	0.70	3.5	0.74	69.1	6	98	0.06	0.94	0.7	0.21	3.27	3.32E+01	10.14	5.7	
85-M Bt2	47–81	1.6	0.1	6.3	0.051	2.06E−07	0.48	2.7	0.81	59.5	4	86	0.05	0.96	0.2	0.31	12.54	9.61E+01	7.67	8.2	
95-M A_P	0–21	5.3	0.5	9.4	0.197	2.05E−06	0.81	3.7	0.64	54.6	7	72	0.08	0.91	1.6	0.19	4.85	21.4	4.41	3.3	245
95-M Bt1	21–54	2.1	0.2	9.5	0.060	3.84E−07	0.57	2.5	0.74	61.8	6	88	0.06	0.94	0.5	0.18	4.56	39.55	8.67	4.4	
95-M Bt2	54–78	1.1	0	0.0	0.030	4.50E−08	0.41	1.8	0.82	58	1	89	0.01	0.99	0.4	0.11	11.33			2.7	
95-M Bt3	78–175	1.1	0	0.0	0.024	1.49E−08	0.33	1.6	0.84	55.7	0	87	0	1.00	0.3	0.16	10.71			3.5	
115-M A_P	0–22	18.6	2.5	13.4	0.630	8.39E−06	0.91	5.4	0.64	70.1	17	79	0.18	0.82	5.2	0.17	3.63	16.37	4.51	3.6	300
115-M Bt1	22–43	7	1	14.3	0.174	1.95E−06	0.77	4.1	0.72	74.3	18	93	0.17	0.84	1.8	0.15	2.74	15.47	5.65	4.0	
115-M Bt2	43–112	2.9	0.3	10.3	0.079	4.82E−07	0.62	3.0	0.80	71.1	12	97	0.11	0.89	0.7	0.12	3.56	1.85E+01	5.20	4.3	
115-M Btg1	112–155	1.3	0	0.0	0.042	8.98E−08	0.37	2.7	0.84	66.2	0	103	0	1.00	0.2	0.26	7			7.0	
115-M Btg2	155–172	2.3	0.2	8.7	0.064	6.72E−07	0.73	1.7	0.75	63.7	22	73	0.23	0.77							
137-M A_P	0–21	6.4	0.7	10.9	0.216	2.08E−06	0.84	3.4	0.72	65.5	7	85	0.08	0.92	2.1	0.14	3.69	16.93	4.59	3.1	270
137-M Bt1	21–55	1.7	0.1	5.9	0.046	2.56E−07	0.58	1.9	0.93	56	2	83	0.03	0.98	0.3	0.23	2.38			6.8	
137-M Bt2	55–90	1.1	0	0.0	0.029	1.00E−07	0.54	1.4	0.81	52.4	1	80	0.01	0.99	0.1	0.45	10.79			8.9	
137-M Bt3	90–132	2.5	0.2	8.0	0.111	8.93E−07	0.83	1.9	0.78	54.2	8	74	0.1	0.90							
150-M A_P	0–21	4.9	0.5	10.2	0.163	1.52E−06	0.84	2.7	0.73	67.1	6	90	0.07	0.94	1.7	0.14	3.91	1.78E+01	4.56	2.9	240
150-M Bt1	21–55	1.5	0.1	6.7	0.038	9.88E−08	0.46	2.0	0.83	51.2	2	75	0.02	0.97	0.2	0.24	4.24	1.59E+01	3.75	9.4	
150-M Bt2	55–102	1	0	0.0	0.023	2.28E−08	0.34	1.5	0.90	48.1	0	75	0	1.00							
150-M Btg1	102–130	1.1	0	0.0	0.038	4.89E−09	0.18	3.2	0.95	40.5	0	62	0	1.00							
150-M Btg2	130–170	1.9	0.1	5.3	0.084	3.59E−07	0.42	4.8	0.88	52.1	25	53	0.32	0.68							
160-M A_P	0–27	18.7	2.5	13.4	0.533	6.75E−06	0.93	3.5	0.62	64.7	11	79	0.13	0.88	10.3	0.14	3.12	14.43	4.63	1.8	230
160-M Bt1	27–45	2.8	0.2	7.1	0.090	4.95E−07	0.77	2.1	0.78	57.1	5	81	0.06	0.94	0.9	0.19	2.83	28.78	10.17	3.1	
160-M Bt2	45–63	1.4	0.1	7.1	0.032	6.93E−08	0.46	1.7	0.86	54.3	1	83	0.01	0.99	0.5	0.13	3.87			2.8	
160-M Btg1	100–157	1.1	0	0.0	0.029	1.36E−08	0.44	1.6	0.98	43.2	0	66	0	1.00							
160-M Btg2	157–175	1.4	0.1	7.1	0.049	8.95E−08	0.63	1.8	0.67	52.5	13	67	0.17	0.84							

The units of the various proxies are: χ, χ_{fd}: 10^{-7} m^3 kg^{-1}; SIRM: 10^{-2} A m^2 kg^{-1}; χ_{arm}: 10^{-6} m^3 kg^{-1}; HIRM: 10^{-4} A m^2 kg^{-1}; Fe_d: g kg^{-1}; Hm and Gt: g kg^{-1}; M_s: 10^{-2} A m^2 kg^{-1}; B_c and B_{cr}: mT; χ/M_s: 10^{-2} m/A; $T_{fd,max}$: K.

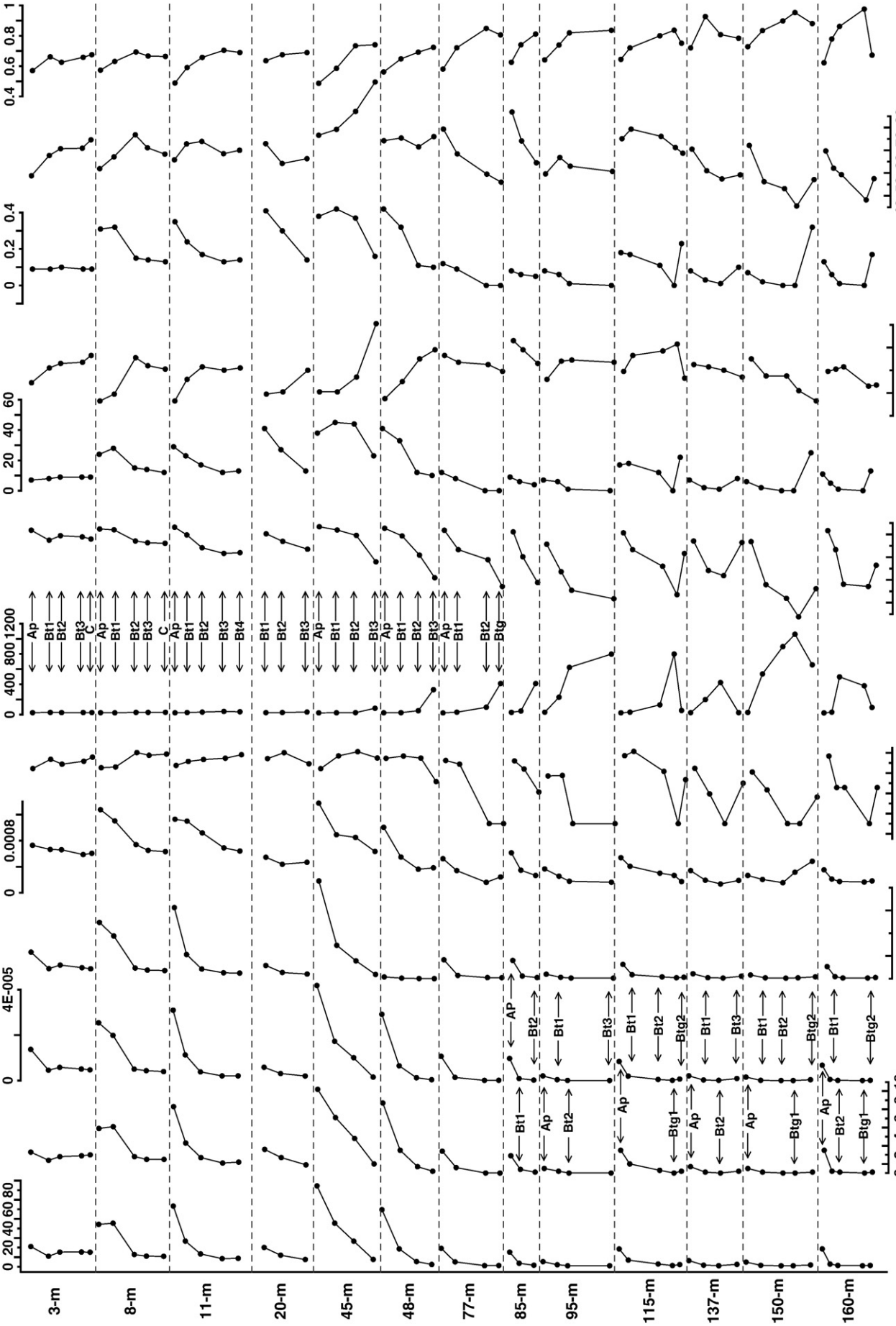

Fig. 1. Variations in different proxies for the Esla soil chronosequence. The dashed lines mark the different terraces. Labels indicate different soil horizons. The hematite (Hm) and goethite (Gt), and Fe_d data are from Torrent et al. (2010b). Labels indicate different soil horizons.

saturation isothermal remanent magnetization, and the remanence obtained by first saturating the sample in 1 T and then applying a back-field of −300 mT, respectively. The S-ratio ($-\mathrm{IRM}_{-300\,\mathrm{mT}}/\mathrm{SIRM}$) was calculated to estimate the relative contributions between the magnetically hard (hematite and goethite) and soft minerals (e.g. magnetite and maghemite) (King and Channell, 1991; Walden et al., 1999). Generally, when the S-ratio approaches 1, magnetite and maghemite dominate the sample. Lower values of the S-ratio indicate the presence of significant amounts of hematite and goethite. However, recent studies revealed that the magnetic properties (including the saturation magnetization and coercivity) of hematite and goethite depend on the degree of Al-for-Fe isomorphous substitution (Liu et al., 2004b). A new parameter, the L-ratio, is then defined as $\mathrm{HIRM}/(0.5\times(\mathrm{SIRM}+\mathrm{IRM}_{-100\,\mathrm{mT}}))$ ($\mathrm{IRM}_{-100\,\mathrm{mT}}$ represents the remanence obtained by first saturating the sample in 1 T and then applying a back-field of −100 mT) to detect the possible variations in the coercivity of the magnetically hard minerals (Liu et al., 2007b). Only when the L-ratio varies little from sample to sample, can the HIRM and S-ratio be interpreted conventionally. All remanences were measured using a 2-G Enterprises cryogenic magnetometer.

The remanence coercivity (B_{cr}) of the bulk samples was determined by the backward remanence acquisition curve using a VFTB system. First, samples were magnetized in a field of 1 T, and then were remagnetized using backfields up to −1 T. Hysteresis loops were also measured by the VFTB system. A Day plot (M_{rs}/M_s versus B_{cr}/B_c) was constructed to determine the domain state of pedogenic ferrimagnets (Day et al., 1977; Dunlop, 2002).

To characterize the magnetic minerals in the samples, the temperature dependent susceptibility ($\chi-T$) was measured using a Kappabridge KLY-3 magnetic susceptibility meter, equipped with a CS-3 furnace, from room temperature to 700 °C in an argon environment (at an Ar flux rate of 50 ml/min).

3. Results

3.1. Depth variations of magnetic properties

The major mineralogical and magnetic properties of the soil chronosequence are summarized in Table 1 and Fig. 1. Overall, for each soil profile, the values of χ, χ_{fd}, ARM, SIRM, and HIRM are all highest in the A horizon, and gradually decrease to the background value down to the lower part of the B horizon (e.g., Bt4) or the C horizon. The strong similar trends among these concentration proxies indicate that the magnetic enhancement is dominantly controlled by increased amounts of ultrafine-grained ferrimagnets (magnetite or maghemite) and antiferromagnetic phases (hematite and goethite). The χ_{fd}% remains relatively constant for the soils on the terraces below 48 m, which are the ones with enhanced magnetic properties. The older soils (terraces>48 m) exhibit weak magnetic properties and the χ_{fd}% values are markedly lower, especially for some Bt and the Btg horizons, which are the ones more affected by the water table.

The B_{cr} values are <30 mT (typical for ferrimagnetic minerals) for the younger soils, but increase up to >1.2 T (typical for Al-goethite) for the B horizons of older soils. This is consistent with the S-ratio for the B horizons, which is >0.7 in the younger soils dominated by the magnetically soft minerals but lower in the older soils, which indicates that magnetic minerals of high coercivity (hematite and/or goethite) are the main magnetic carriers.

As indicated before, the L-ratio has been used as the coercivity proxy for antiferromagnetic minerals (hematite and goethite) (Liu et al., 2007b). The downward increase trend in the L-ratio in the older soils is consistent with the fact that the magnetically hard mineral (goethite) is dominant because hematite has been reductively dissolved (Torrent et al., 2010b). It must be noted that the χ value of the clay of the B horizons containing no hematite ($1–1.5\times10^{-7}$ m^3 kg^{-1}) is consistent with contents of about 6–9% of goethite in those samples because the χ values for this mineral are in the region of 10×10^{-7} m^3 kg^{-1} (Peters and Dekkers, 2003). In contrast, in younger soils, the hematite content is higher, and the overall coercivity of the antiferromagnetic assemblage is thus lower.

3.2. Low-temperature measurements ($\chi_{fd}(T)$ curves)

The $\chi_{fd}(T)$ curves for the magnetically enhanced soil horizons are shown in Fig. 2. All curves exhibit similar patterns. With increasing temperature, χ_{fd} values gradually increase. However, the χ_{fd} values maximize at various temperatures ($T_{\chi fd,max}$) for different horizons. For example, for samples from the 3 m terrace, $T_{\chi fd,max}$ is well below 300 K. In contrast, the 8 m Ap horizon has a $T_{\chi fd,max}$ apparently >300 K. Clearly, for the 8 m terrace, $T_{\chi fd,max}$ gradually decreases from >300 K for the upper Ap horizon down to <300 K for the underlying B horizons. Such a pattern can also be observed for samples from the 45 m terrace.

Assuming that a single strongly magnetic phase dominates the χ_{fd} signal, the χ_{fd}–T curves can be translated to the grain size distribution of ferrimagnetic particles (Liu et al., 2005b; Egli, 2009). However, at temperatures below the Verwey transition (~120–122 K), coarse-grained magnetite and titanomagnetite also exhibit frequency-dependent behaviour due to reorganization of domain walls (Simša et al., 1985; Radhakrishnamurthy and Likhite, 1993; Moskowitz et al., 1998; Skumryev et al., 1999; Kosterov, 2003; Lagroix et al., 2004). In addition, nano-sized antiferromagnetic minerals (e.g., ferrihydrite; Guyodo et al., 2006) can also contribute to the low-temperature (<100 K) χ_{fd} due to their strong magnetization caused by the uncompensated surface spins. In contrast, Michel et al. (2010) affirmed that ferrihydrite is strongly magnetic at lower temperatures and the disordered surface spins of ferrihydrite decrease rather than increase its bulk M_s. Nevertheless, for our cases, the latter two mechanisms do not affect the interpretation of the χ_{fd} peak above the Verwey transition. In addition, because the grain size distribution plays a more important role than the magnetic anisotropy, to the first order, $T_{fd\text{-}max}$ corresponds to the average unblocking temperature, which is generally proportional to the mean particle volume provided the anisotropy constant is invariable (Gittleman et al., 1974; Khater et al., 1987; El-Hilo et al., 1992; Liu et al., 2005b).

Confined by the maximum measurement temperature, one more disadvantage of this method is that it cannot be applied to particles in the stable single domain region with the average unblocking temperatures much higher than the room-temperature. Fortunately, unlike the results for the Chinese loess/paleosol sequences, $T_{fd\text{-}max}$ for most of the soils studied here lies generally below room temperature (Table 1, Fig. 2), which provides an ideal opportunity to check for systematic changes in the soil profile. The systematic changes in $T_{fd\text{-}max}$ indicate that the average grain size of the newly formed ferrimagnetic particles systematically changes with depth in the profile.

3.3. Relationships between mineralogical and magnetic properties

Because the M_s of antiferromagnetic minerals (hematite and goethite) is about two orders of magnitude lower than that of ferrimagnetic minerals, M_s for the bulk samples provides thus an

Fig. 2. Temperature-dependent of χ_{fd} curves for magnetically enhanced horizons of the Esla soil chronosequences. The thick curves are the third-order polynomial trends fitted to the data between 5 and 300 K. Except for the Ap horizons, data for samples above the 48 m terrace are not included because no accurate measurements were obtained for these samples with extremely low magnetic properties.

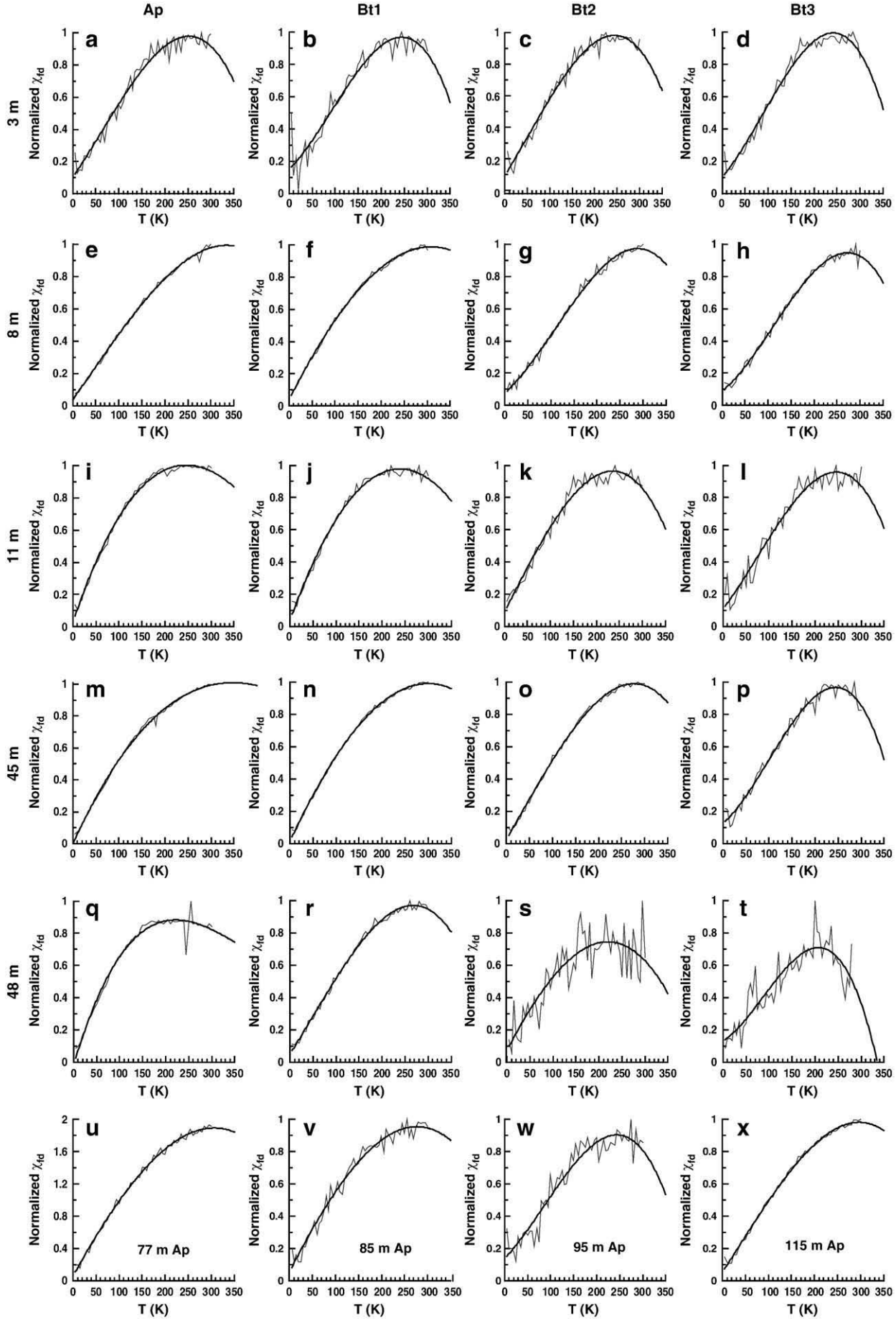
Ap
Bt1
Bt2
Bt3
3 m
8 m
11 m
45 m
48 m
a
b
c
d
e
f
g
h
i
j
k
l
m
n
o
p
q
r
s
t
u
v
w
x
Normalized χ_{fd}
T (K)
77 m Ap
85 m Ap
95 m Ap
115 m Ap

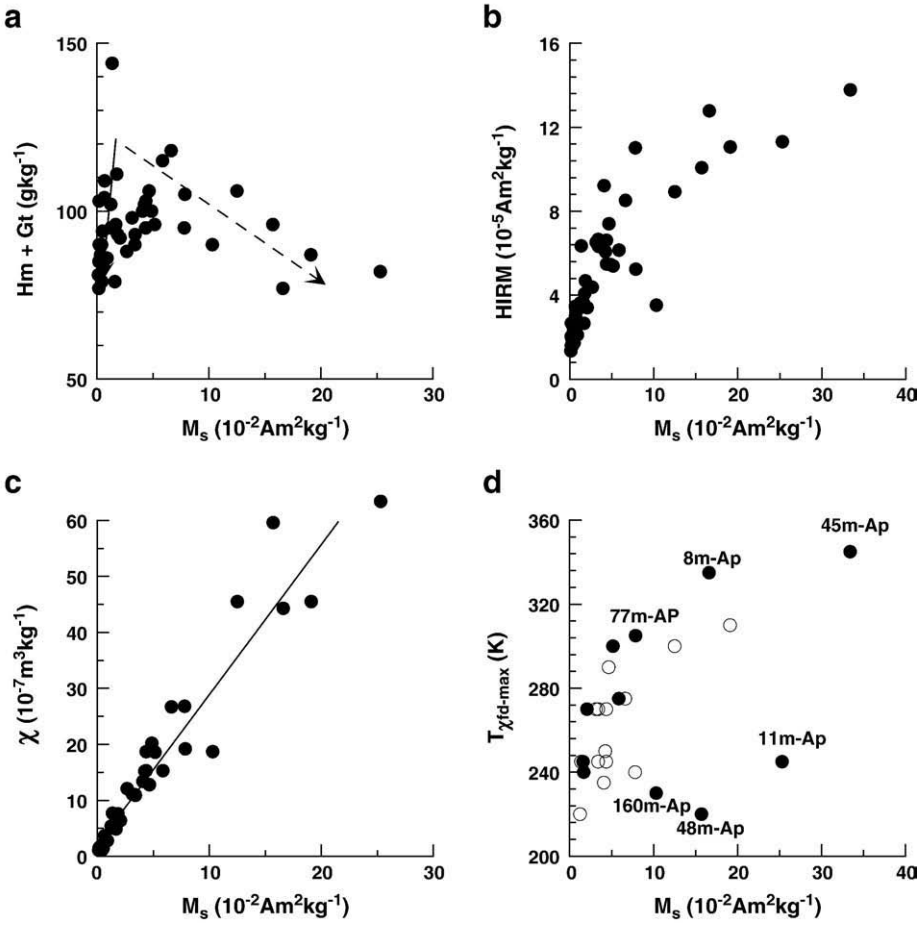

Fig. 3. Variations in different proxies with respect to the saturation magnetization. (a) The mass concentration of hematite (Hm) and goethite (Gt); (b) HIRM; (c) χ; and (d) $T_{\chi fd\text{-}max}$. The solid and dashed lines in (a) indicates that the correlation can be fitted by two linear trends. In (c), the linear trend yields a slope of about 20×10^{-6} m A^{-1}, which strongly indicates the presence of superparamagnetic particles. The solid and open circles in (d) indicate samples from the Ap and the other horizons, respectively. In addition, the open circles in (d) also indicate samples without effects from greying.

estimate of the absolute mass concentration of the ferrimagnetic minerals, and is independent of the grain size distribution. With increasing M_s, the mass concentration of hematite + goethite increases, and then decreases (Fig. 3a). In contrast, HIRM is positively correlated with M_s, which indicates that hematite and ferrimagnetic minerals are inherently correlated (Fig. 3b). The ratio of χ and M_s is an indicator for SP particles. The slope for the linear correlation between χ and M_s is about 27×10^{-6} m A^{-1}, which is about 4–5 times higher than the value ($\sim6\times10^{-6}$ m A^{-1}) for relatively coarse-grained ferrimagnetic particles (Fig. 3c). This further demonstrates that SP particles are abundant in these samples. $T_{fd\text{-}max}$ shows a good positive correlation with M_s if the three data points corresponding to the Ap horizon of the soils on the 11-, 48- and 160-m levels are excluded (Fig. 3d).

There is a statistically linear correlation between χ_{fd} and χ (Fig. 4a), which indicates that the bulk χ is controlled by the fine-grained magnetic particles. However, the relationship between χ_{fd}% and χ shows a subtle feature for the more magnetically enhanced samples. Clearly, the relationship between χ_{fd}% and χ is described better by a two-line fit: for $\chi<\sim6\times10^{-7}$ m^3 kg^{-1}, these two proxies are positively correlated whereas χ_{fd}% decreases from ~14% to ~11% for higher χ values (Fig. 4b). The plot of the L-ratio against χ also follows a two-line pattern (Fig. 4c): a steep decrease (~0.98 down to ~0.7 for $\chi<\sim6\times10^{-7}$ m^3 kg^{-1}) is followed by a more gentle decrease (down to ~0.5 for $\chi=\sim80\times10^{-7}$ m^3 kg^{-1}).

Traditionally, χ_{fd} and χ_{fd}% were used to identify the presence of SP ferrimagnets in samples (Stephenson, 1971; Mullins and Tite, 1973; Mullins, 1977; Oldfield et al., 1985; Dearing et al., 1996) and thus determine the degree of pedogenesis. However, such a rationale is valid only for a fixed GSD of the fine-grained particles (Liu et al., 2005b). Theoretically, χ_{fd} is sensitive only to a narrow grain size window located at the SP/SD threshold (~20–25 nm) (Oldfield et al., 1985; Worm, 1998), and thus cannot register the presence of the particles far from the SP/SD threshold (Liu et al., 2005b). Generally, we expect higher χ_{fd}% values when the concentration of SP particles increases, e.g., for the incipient soils for the Chinese loess–paleosol sequences (Liu et al., 2003). Further studies showed that χ_{fd}% reflects mostly the GSD of the ferrimagnets, a wider GSD resulting in a lower χ_{fd}% value (Worm, 1998).

The χ_{fd}% for the Esla soils shows a more complicated behaviour (Fig. 4b). Values of $<\sim6\times10^{-7}$ m^3 kg^{-1} for the bulk χ correspond to horizons affected by waterlogging and reduction of Fe oxides (Torrent et al., 2010b). For these samples, χ and $\chi_{fd\%}$ are positively correlated, which is consistent with the idea that the loss of SP and SD maghemite particles resulted in reduction of both $\chi_{fd\%}$ and χ_{fd}. For $\chi>\sim6\times10^{-7}$ m^3 kg^{-1}, a negative correlation between χ_{fd}% and χ is observed (i.e. the concentration and the peak size of pedogenic maghemite particles both increase with increasing magnetic enhancement). The effects the GSD and the peak grain size on χ_{fd}% have been well studied by Worm (1998). For a relatively fixed grain size distribution width, when the average grain size is finer than the SP/SD threshold, an increase of the peak size will result in an increase in χ_{fd}%. However, when the peak size lies above the SP/SD threshold, χ_{fd}% will decrease with increasing grain size. With this model, the negative

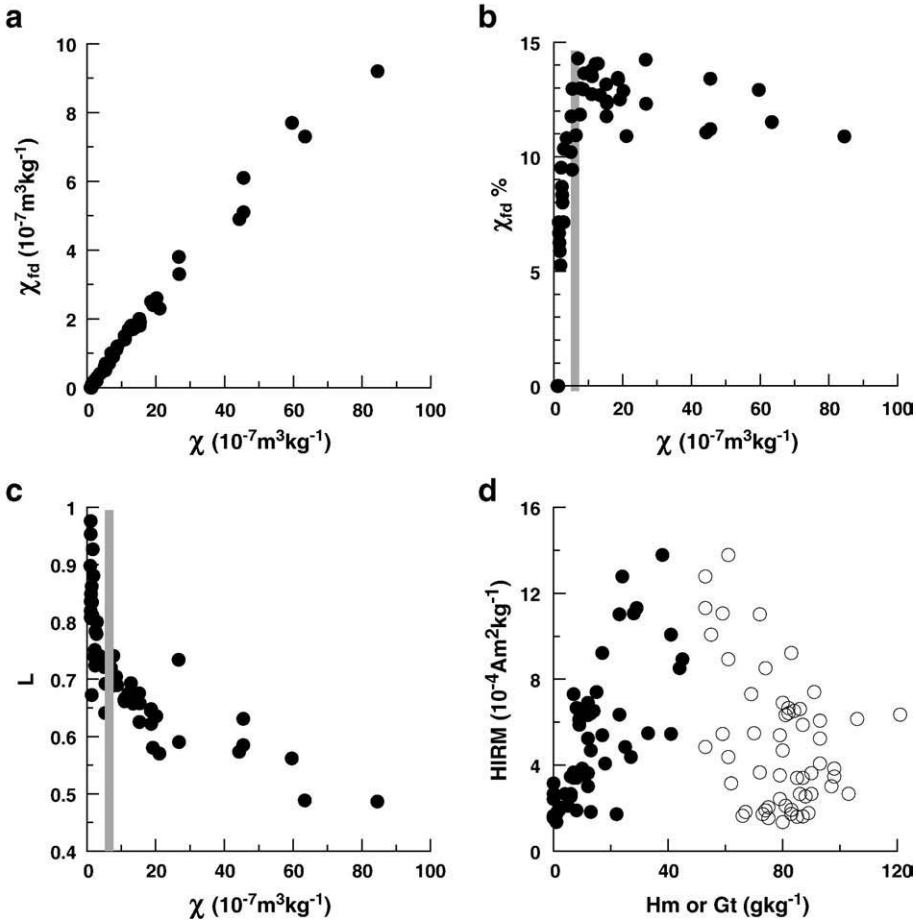

Fig. 4. Relationships between (a) χ_{fd} and χ, (b) χ_{fd}% and χ, (c) L and χ, and (d) HIRM and the mass concentration of hematite (solid circles) and goethite (open circles). The grey bar indicates the boundary for two segments to fit the whole trend. The dashed line in (a) was fitted to data with values $\chi < 30\times10^{-7}$ m^3 kg^{-1}. Clearly, when $\chi < 30\times10^{-7}$ m^3 kg^{-1}, data points gradually depart from the linear trend.

correlation between χ_{fd}% and the bulk χ can be reasonably explained by the gradual increase of grain size above the SP/SD threshold, and thus caution should be exerted when interpreting the paleoenvironmental significance of χ_{fd}% in future studies.

The correlations between HIRM and the hematite and goethite concentrations can be used to determine which antiferromagnetic mineral controls the HIRM. Results show (Fig. 4d) that HIRM is positively correlated to the hematite, but inversely to the goethite concentration. The y-axis intercept for the correlation between HIRM and the hematite concentration is $\sim 2\times10^{-4}$ A m^2 kg^{-1}, which should be carried by goethite. Therefore, hematite rather than goethite dominates the HIRM values. This can be ascribed to the relatively high Al-for-Fe substitution in the goethite present in these soils (Torrent et al., 1980). This results in Néel temperatures close to or below room temperature, and in turn substantial reduction of the ability of goethite to carry remanence (Liu et al., 2004).

3.4. High-temperature measurements (χ–T curves)

The χ–T cooling curves of the different horizons show a similar pattern (Fig. 5). The room-temperature χ values after the heating/cooling cycle are higher than those for the raw samples. This strongly indicates that strongly magnetic minerals were formed upon heating. The Curie temperature of ~580 °C and the unblocking temperature of ~350 °C for the cooling curve further indicate that fine-grained magnetites in the single-domain grain size region were formed during the thermal treatment.

The χ–T warming curves exhibit complicated features. For the Ap horizon (Fig. 5a), χ gradually increased with increasing temperature up to ~200 °C, exhibited a sharp peak between 200 and 240 °C, and then decreased before exhibiting a weaker peak at ~500 °C. The Curie temperature of ~580 °C indicates that magnetite was present. For the Bt horizons, both χ peaks were gradually smeared and, for the Bt3 horizon, the second χ peak completely disappeared.

The stepwise χ–T curves (Fig. 6) show gradual increase in χ when temperature is below ~240 °C (Fig. 6a and b). The cooling curve is relatively stable, and thus such an increase dominantly reflects the gradual unblocking of SD particles. The slight increase in the room-T χ for the 200 °C could be due to the partial dehydration of goethite to hematite. After the 330 °C thermal treatment (Fig. 6c and d), the cooling curve lies well below the warming one. This pattern has been widely interpreted by the transformation of metastable maghemite into weakly magnetic hematite upon heating (Sun et al., 1995; Oches and Banerjee, 1996; Florindo et al., 1999). Above 400 °C, the cooling curve lies above the heating curve; this indicates that the thermal treatment above 400 °C resulted in neoformation of strongly magnetic minerals (Fig. 6f).

3.5. Day plot

On the basis of theoretical simulation, Dunlop (2002a,b) reinterpreted the Day plot initially suggested by Day et al. (1977). There are some ambiguities in interpreting the Day plot. The model of Dunlop (2002a,b) relied on a simple mixture model without considering the

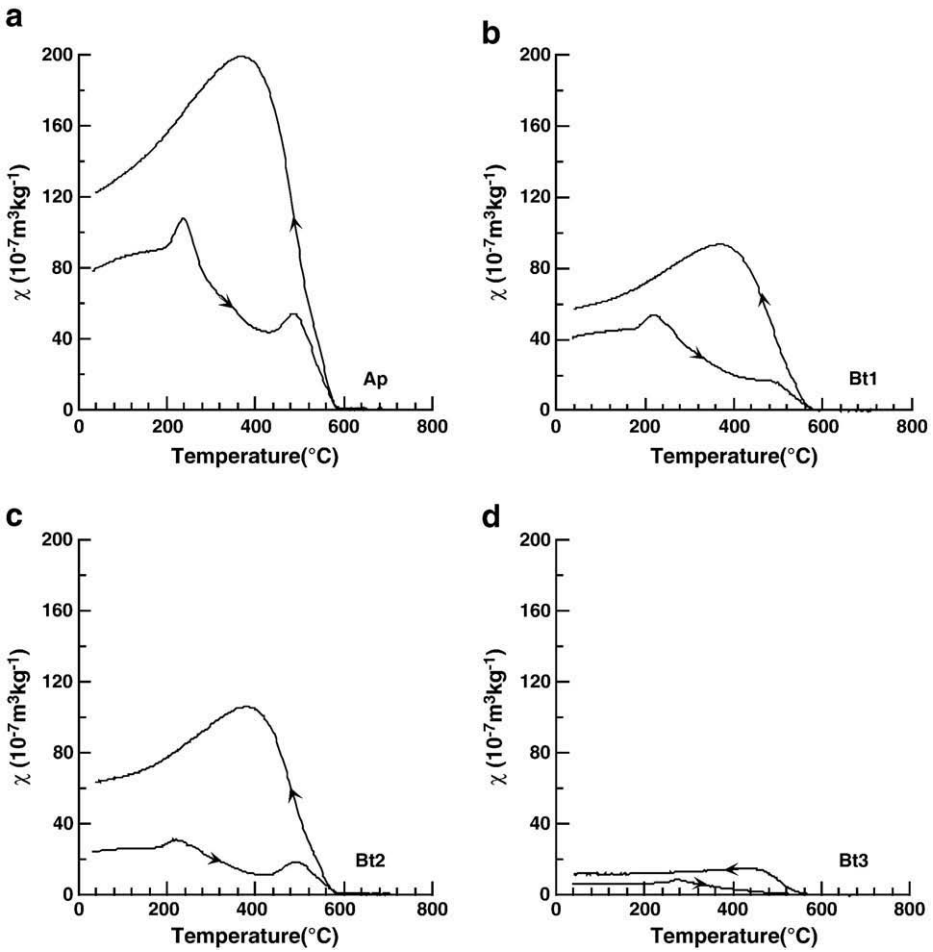

Fig. 5. Temperature dependence of magnetic susceptibility curves for different horizons from the soil at the 45 m terrace. Note that the cooling curves lie above the warming ones. Arrows indicate the heating/cooling processes.

grain size distribution of magnetic particles. Therefore, the SP/SD mixing lines cannot be quantitatively applied to natural samples, which generally exhibit a wide grain size distribution. Nevertheless, the most successful indication from the model of Dunlop (2002a,b) is that the plots just above the traditional MD grain size region indicate a mixture of SD and SP particles. Our results (Fig. 7) support the contention that the magnetically enhanced horizons are dominated by a SP + SD mixture, in contrast with the Chinese loess paleosols, for which the Day plot data points lie in the pseudo-single domain (PSD) region (Liu et al., 2003).

4. Discussion

The exact mechanism for the magnetic enhancement of the A and B horizons is still under discussion, specifically on the formation pathway of maghemite. The first mechanism involves an indirect pathway. First, fine-grained magnetite is formed via inorganic (Maher and Taylor, 1988) or bacterially mediated pathways (Lovley et al., 1987; Fassbinder et al., 1993), and is then oxidized into maghemite at the soil temperature (Verosub et al., 1993). The second mechanism bases on the fact the maghemite can be directly formed via mineral transformation chain from ferrihydrite to maghemite, and then to hematite under an oxidizing environment (Barrón and Torrent, 2002; Torrent et al., 2006). Michel et al. (2010) further revealed that the intermediate highly magnetic phase during the transformation of ferrihydrite to hematite is ordered ferrihydrite. The relationship between ordered ferrihydrite and maghemite needs further studies, but the gradual growth of grain sizes of magnetic phases is obvious.

In natural environments, it is difficult to observe these dynamic processes because for most cases, the system has evolved into a relatively mature state. For example, the average grain size of the pedogenic ferrimagnets is rather stable and is independent of the degree of pedogenesis (Liu et al., 2005b; Geiss and Zanner, 2006; Nie et al., 2009). Therefore, it is critical to observe the intermediate states to accurately understand how pedogenic ferrimagets were dynamically formed in natural environments.

Based on the diffuse reflectance spectroscopy measurements (Torrent et al., 2010b) and the rock magnetic measurements in this study, the magnetic assemblage in the Esla soil chronosequence includes hematite, goethite and maghemite. On the basis of the thermal treatment, magnetite could also be present, but it may be formed during the thermal treatment. Regardless of the presence of magnetite, the fine-grained magnetic particles are dominated evidently by the low unblocking temperature <300 K, which corresponds to the grain size <~20–25 nm (Liu et al., 2005b). For such fine-grained particles in a natural oxidating environment, the most stable phase is maghemite rather than magnetite.

Although the magnetic properties are determined by the ferrimagnetic minerals (e.g. maghemite) for the magnetically enhanced soil horizons, hematite and goethite play, in terms of mass, a dominant role in the pedogenic processes. Ferrihydrite is the precursor for hematite in soil environments, its transformation involving aggregation–dehydration–rearrangement processes (Cornell and Schwertmann, 2003). Laboratory experiments have shown that when some ligands are adsorbed on the ferrihydrite particles, the ferrihydrite–hematite transformation goes through an intermediate, metastable ferrimagnetic

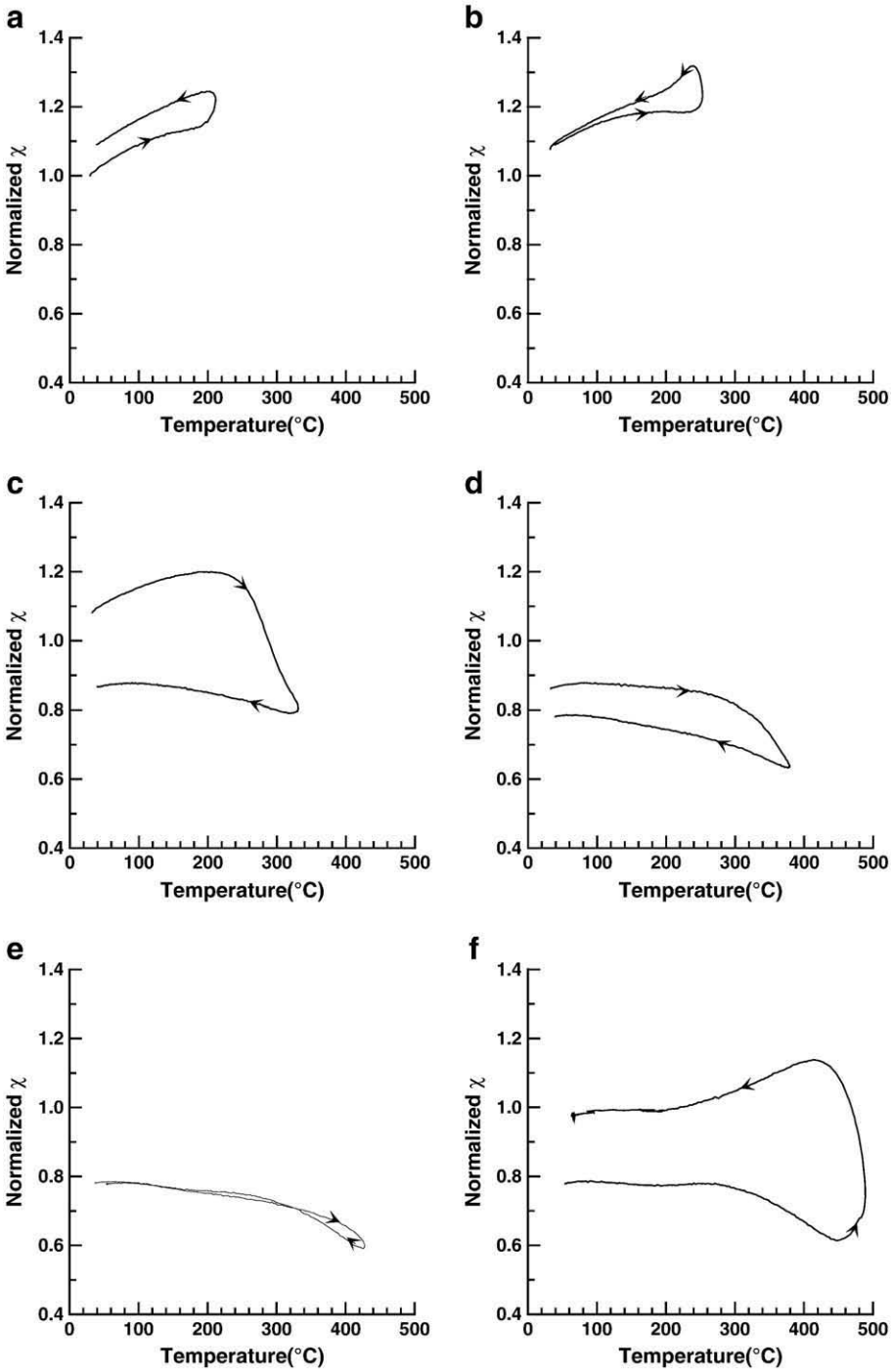

Fig. 6. Stepwise temperature dependence of magnetic susceptibility curves for the Ap horizon of the soil profile at the 45 m terrace. All curves are normalized by the initial susceptibility for the raw sample.

nanophase (Barrón and Torrent, 2002; Barrón et al., 2003), the particles of which grow in size before its transformation into hematite (Liu et al., 2008). On the basis of mineralogical and magnetic data of different hematite-containing soils, several authors have suggested this phase, or the maghemite derived thereof, to constitute the bulk of the pedogenic ferrimagnets (Torrent et al., 2006; 2007, 2010a,b). The Esla soils are acidic, which ensures a strong interaction between the positively charged Fe oxides and various ligands present in the soil solution (e.g. phosphate, citrate and malate) (Geelhoed et al., 1998) and, therefore, the possible transformation of ferrihydrite into maghemite and hematite.

If this model is valid, the concentration of the newly-formed ferrimagnetic particles and their average grain size will both increase before the final transformation into hematite. Our results show that, M_s and $T_{\chi fd\text{-}max}$ are positively correlated if the data points for three Ap horizons are excluded. This strongly indicates that the more magnetically enhanced horizons contain relatively coarser-grained magnetic particles. The model also predicts that the concentration of hematite and any proxy for the concentration of the pedogenic ferrimagnets should be positively correlated, as is the case with different soils — including those studied here (Torrent et al., 2006, 2007, 2010a,b).

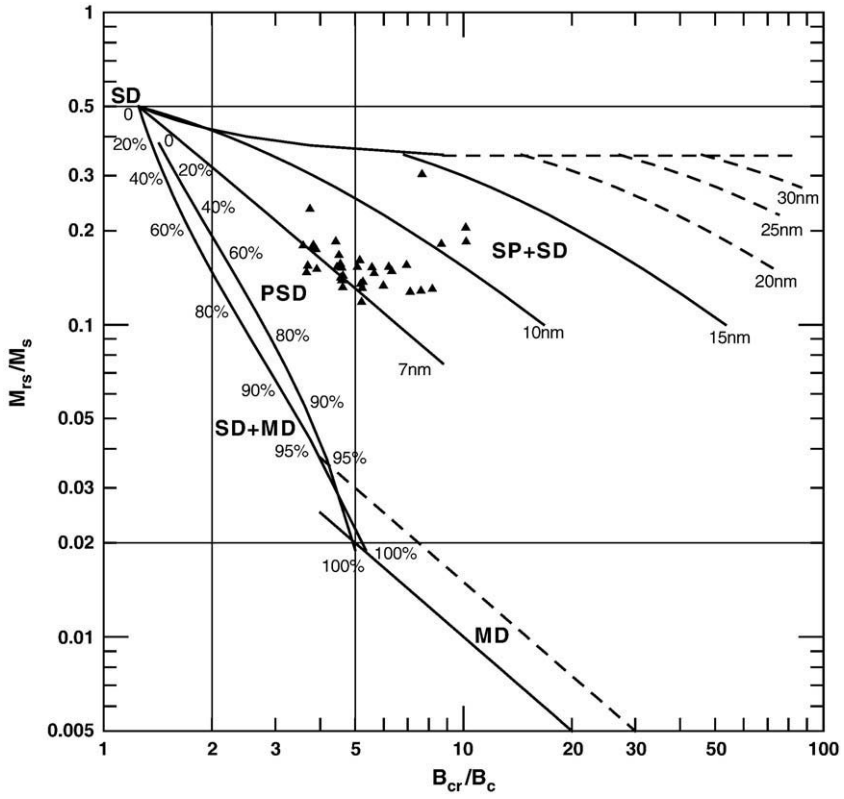

Fig. 7. The Day plot for the Esla soil chronosequence. The interpretation framework is after Dunlop (2002a,b). Apparently, the data points follow the SP + SD mixture lines.

More specifically, the correlation between the average grain size and concentration of pedogenic ferrimagnets can be divided into two stages (Fig. 3d). During the first stage, the average grain size ($T_{\chi fd\text{-}max}$) and the concentration (M_s) both increase, which corresponds to the initial growth of the particles. Therefore, at this stage, the particle growth also plays an important role in magnetic enhancement. During the second stage, particle size remains relatively stable; therefore, the corresponding magnetic enhancement is mainly caused more by increases in concentration. This model is consistent with the laboratory observation (Liu et al, 2008) that hematite is produced via an intermediate ferrimagnetic phases through aging of phosphated ferrihydrite (P/Fe atomic ratio = 0.03) at 150 °C for 120 days. In addition, the average unblocking temperature for the stable stage is just above 300 K, which corresponds to the grain size of ~25 nm for maghemite.

The initial stage can be alternatively interpreted as the selective dissolution of fine-grained particles resulting in decreases in both the grain size and the concentration of ferromagnetic particles upon gleying. However, this mechanism can be excluded because the gleying process affected samples only above the 48 m terrace. The positive correlation between $T_{\chi fd\text{-}max}$ and M_s still holds for samples from the younger terraces below 48 m (open circles in Fig. 3d).

The M_s and $T_{\chi fd\text{-}max}$ values for some Ap horizons (Fig. 3d) are difficult to interpret. They could reflect the inherent complexity of the soil environment for the Ap horizon, mostly the type and concentration of organic matter in the undisturbed soil, in turn dependent on the type of natural vegetation (that has changed during the Quaternary) and pH (dependent on the parent alluvium). The soils are polygenic, and are controlled by various time-dependent soil forming factors (e.g. climate and organisms). In addition, part of the clay of the Ap horizon was translocated to the B horizons, which could determine that the Fe oxides associated with the silicate clays remaining in the Ap horizons were different from those associated with the clays translocated to the Bt horizons. The relatively simple correlation between grain size and concentration of pedogenically-produced maghemite for the Bt horizons indicates that, in contrast to the Ap horizons, only a few factors control the formation of ferrimagnets in the Bt horizons.

Unlike the Esla soils, the pedogenic ferrimagnets in Chinese loess/paleosol sequences since the late Pleistocene show a rather uniform grain size distribution, which is independent of the degree of pedogenesis (Liu et al., 2005b). Several reasons argue for this difference. One is that the Chinese loess was calcareous. Thus, the formation of ferrimagnets was possible only after calcium carbonate was dissolved and leached from the surface horizon (because the high pH typical of a calcareous medium hinders mineral weathering) in periods in which the rate of accumulation of new calcareous aeolian sediments was not so high to prevent decalcification of the topsoil. Pedogenesis might then conform to a steady state in which the chemical environment of the topsoil did not change substantially with time (e.g. pH was likely to lie in the neutral to slightly acidic range because of the balance between carbonate leaching and the additions of calcareous dust). Such constant environment would favor a constant GSD for the neoformed ferrimagnets. With the onset of a period of intense aeolian activity the soils were rapidly buried and thus "frozen" in terms of evolution and so the properties of their ferrimagnets did not undergo further change. By contrast, the Esla soils have acidic pH, which favors weathering, and have been exposed at the surface all the time. For this reason, they are palimpsests that have recorded the effects of the successive environments on the weathering of the Fe-bearing minerals and the subsequent formation and transformation of the different Fe oxides. Under these conditions the GSD of the ferrimagnets is likely to depend on soil age (i.e. terrace height).

5. Conclusions

The magnetic enhancement of soil is generally due to the neoformation of ferrimagnets through pedogenesis. Previous studies showed that grain size distribution of these pedogenic ferrimagnets for paleosols is rather uniform, and independent of the degree of pedogenesis. In contrast, this study revealed that, except for the Ap

horizons, there is a positive correlation between the average grain size and the concentration of pedogenic ferrimagnets for the Bt horizons of the Esla soil chronosequence. This is consistent with the idea of the gradual formation of maghemite and hematite via the precursor ferrihydrite. Thus, this study provides a direct observation of the dynamic formation of pedogenic ferrimagnets in natural soils. Such a simple correlation for the Bt horizon further indicates that only a few soil factors control the formation of ferrimagnets in these underlying horizons. Moreover, supported by the theoretical simulation, variations in the distribution and average grain size of the pedogenic ferrimagnets both strongly affect the frequency dependence of magnetic susceptibility. Therefore, caution should be exerted when linking the frequency dependence of magnetic susceptibility solely to the grain size distribution of these fine-grained magnetic particles. Although the conclusion from this study is made from a single chronosequence in a specific environmental context, we believe that it can be generalized to broader environments, but further studies from other regions are essentially needed.

Acknowledgements

This study was supported by the National Natural Science Foundation of China (grants 40974036 and 40821091) and the CAS/SAFEA International Partnership Program for Creative Research Teams. Q.S. Liu acknowledges further supports from the 100-talent Program of the Chinese Academy of Sciences. Y.L. Su further thanks supports from NSFC 40874033. J. Torrent and V. Barrón were partly supported by Spain's Ministerio de Educación y Ciencia, Project AGL2006-10927, and FEDER funds.

References

Barrón, V., Torrent, J., 1987. Origin of red-yellow mottling in a Ferric Acrisol of southern Spain. Z. Pflanzenernäh. Bodenk. 150, 308–313.
Barrón, V., Torrent, J., 2002. Evidence for a simple pathway to maghemite in Earth and Mars soils. Geochim. Cosmochim. Acta 66, 2801–2806.
Barrón, V., Torrent, J., de Grave, E., 2003. Hydromaghemite, an intermediate in the hydrothermal transformation of 2-line ferrihydrite into hematite. Am. Mineral. 88, 1679–1688.
Birkeland, P.W., 1984. Soils and Geomorphology. Oxford Univ, Press, New York.
Blundell, A., Dearing, J.A., Boyle, J.F., Hannam, J.A., 2009. Controlling factors for the spatial variability of soil magnetic susceptibility across England and Wales. Earth Sci. Rev. 95, 158–188.
Bockheim, J.G., 1980. Solution and use of chronofunctions in studying soil development. Geoderma 24, 71–85.
Chen, T.H., Xu, H.F., Xie, Q.Q., Chen, J., Ji, J.F., Lu, H.Y., 2005. Characteristics and genesis of maghemite in Chinese loess and paleosols: mechanism for magnetic susceptibility enhancement in paleosols. Earth Planet. Sci. Lett. 240, 790–802.
Cornell, R.M., Schwertmann, U., 2003. The Iron Oxides, 2nd. Ed. Wiley-WCH, Weinheim, Germany.
Day, R., Fuller, M., Schmidt, V.A., 1977. Hysteresis properties of titanomagnetites: grain size and composition dependence. Phys. Earth Planet. Inter. 13, 260–267.
Dearing, J.A., Dann, R.J.L., Hay, K., Lees, J.A., Loveland, P.J., Maher, B.A., O'Grady, K., 1996. Frequency-dependent susceptibility measurements of environmental materials. Geophys. J. Int. 124, 228–240.
Deng, C.L., Vidic, N.J., Verosub, K.L., Singer, M.J., Liu, Q.S., Shaw, J., Zhu, R.X., 2005. Mineral magnetic variation of the Jiaodao Chinese loess/paleosol sequence and its bearing on long-term climatic variability. J. Geophys. Res. 110, B03103. doi:10.1029/2004JB003451.
Deng, C.L., Shaw, J., Liu, Q.S., Pan, Y.X., Zhu, R.X., 2006. Mineral magnetic variation of the Jingbian loess/paleosol sequence in the northern Loess Plateau of China: implications for Quaternary development of Asian aridification and cooling. Earth Planet. Sci. Lett. 241, 248–259.
Dunlop, D.J., 2002a. Theory and application of the day plot (M_{rs}/M_s versus H_{cr}/H_c), 1. Theoretical curves and tests using titanomagnetite data. J. Geophys. Res. 107, B32056. doi:10.1029/2001JB000486.
Dunlop, D.J., 2002b. Theory and application of the day plot (M_{rs}/M_s versus H_{cr}/H_c). 2. Application to data for rocks, sediments, and soils. J. Geophys. Res. 107, B32057. doi:10.1029/2001JB000486.
Egli, R., 2009. Magnetic susceptibility measurements as a function of temperature and frequency I: inversion theory. Geophys. J. Int. 177, 395–420.
El-Hilo, M., O'Grady, K., Chantrell, R.W., 1992. Susceptibility phenomena in a fine particle system I. Concentration dependence of the peak. J. Magn. Magn. Mater. 114, 295–306.
Evans, M.E., Heller, F., 1994. Magnetic enhancement and palaeoclimate: study of a loess/palaeosol couplet across the Loess Plateau of China. Geophys. J. Int. 117, 257–264.
Fassbinder, J.W.E., Stanjek, H., Vali, H., 1993. Occurrence of magnetic bacteria in soil. Nature 343, 161–163.
Florindo, F., Zhu, R.X., Guo, B., Yue, L.P., Pan, Y.X., Speranza, F., 1999. Magnetic proxy climate results from the Duanjiapo loess section, southernmost extremity of the Chinese loess plateau. J. Geophys. Res. 104, 645–659.
Geelhoed, J.S., Hiemstra, T., van Riemsdijk, W.H., 1998. Competitive interaction between phosphate and citrate on goethite. Environ. Sci. Technol. 32, 2119–2123.
Geiss, C.E., Zanner, C.W., 2006. How abundant is pedogenic magnetite? Abundance and grain size estimates for loessic soils based on rock magnetic analyses. J. Geophys. Res. 111, B12S21. doi:10.1029/2006JB004564.
Gittleman, J.I., Abelas, B., Bozowski, S., 1974. Superparamagnetism and relaxation effects in granular Ni–SiO_2 and Ni–Al_2O_3 films. Phys. Rev. B9, 3891–3897.
Guyodo, Y., Banerjee, S.K., Penn, R.L., Burleson, D., Berquo, T.S., Seda, T., Solheid, P., 2006. Magnetic properties of synthetic six-line ferrihydrite nanoparticles. Phys. Earth Planet. Inter. 154, 222–233.
Han, J.M., Lu, H.Y., Wu, N.Q., Guo, Z.T., 1996. The magnetic susceptibility of modern soils in China and its paleoclimate reconstruction. Stud. Geophys. Geod. 40, 262–275.
Heller, F., Liu, T.S., 1986. Palaeoclimatic and sedimentary history from magnetic susceptibility of loess in China. Geophys. Res. Lett. 13, 1169–1172.
Heller, F., Shen, C.D., Beer, J., Liu, X.M., Liu, T.S., Bronger, A., Suter, M., Bonani, G., 1993. Quantitative estimations of pedogenic ferrimagnetic formation in Chinese loess and palaeoclimatic implications. Earth Planet. Sci. Lett. 114, 385–390.
Huggett, R.J., 1998. Soil chronosequences, soil development, and soil evolution: a critical review. Catena 32, 155–172.
Jenny, H., 1941. Factors of Soil Formation. McGraw-Hill, New York.
Jenny, H., 1980. The Soil Resource — Origin and Behavior. Springer, New York.
Kelly, E.F., Yonker, C.M., 2005. Factors of soil formation/time. In: Hillel, D. (Ed.), Encyclopedia of Soils in the Environment. Elsevier, Amsterdam, pp. 536–539.
Khater, A., Ferre, J., Meyar, P., 1987. Spin-cluster theory in magnetic materials and applications to spin glasses. J. Phys. 20, 1857–1865.
King, J.W., Channell, J.E.T., 1991. Sedimentary magnetism, environmental magnetism and magnestostratigraphy. Rev. Geophys. 9, 358–370.
Kosterov, A., 2003. Low-temperature magnetization and AC susceptibility of magnetite: effect of thermomagnetic history. Geophys. J. Int. 154, 58–71.
Kukla, G., Heller, F., Liu, X.M., Xu, T.C., Liu, T.S., An, Z.S., 1988. Pleistocene climates in China dated by magnetic susceptibility. Geology 16, 811–814.
Lagroix, F., Banerjee, S.K., Jackson, M.J., 2004. Magnetic properties of the Old Crow tephra: identification of a complex iron titanium oxide mineralogy. J. Geophys. Res. 109, B01104. doi:10.1029/2003JB002678.
Liu, Q.S., Banerjee, S.K., Jackson, M.J., Chen, F.H., Pan, Y.X., Zhu, R.X., 2003. An integrated study of the grain-size-dependent magnetic mineralogy of the Chinese loess/paleosol and its environmental significance. J. Geophys. Res. 108, B92437. doi:10.1029/2002JB002264.
Liu, Q.S., Banerjee, S.K., Jackson, M.J., Chen, F.H., Pan, Y.X., Zhu, R.X., 2004a. Determining the climatic boundary between the Chinese loess and palaeosol: evidence from aeolian coarse-grained magnetite. Geophys. J. Int. 156, 267–274.
Liu, Q.S., Torrent, J., Yu, Y.J., Deng, C.L., 2004b. Mechanism of the parasitic remanence of aluminous goethite (alpha-(Fe, Al)OOH). J. Geophys. Res. 109, B12106. doi:10.1029/2004JB003352.
Liu, Q.S., Banerjee, S.K., Jackson, M.J., Deng, C.L., Pan, Y.X., Zhu, R.X., 2005a. Inter-profile correlation of the Chinese loess/paleosol sequences during Marine Oxygen Isotope Stage 5 and indications of pedogenesis. Quat. Sci. Rev. 24, 195–210.
Liu, Q.S., Torrent, J., Maher, B.A., Yu, Y.J., Deng, C.L., Zhu, R.X., Zhao, X.X., 2005b. Quantifying grain size distribution of pedogenic magnetic particles in Chinese loess and its significance for pedogenesis. J. Geophys. Res. 110, B11102. doi:10.1029/2005JB003726.
Liu, Q.S., Deng, C.L., Torrent, J., Zhu, R.X., 2007a. Review of recent developments in mineral magnetism of the Chinese loess. Quat. Sci. Rev. 26, 368–385.
Liu, Q.S., Roberts, A.P., Torrent, J., Horng, C.-S., Larrasoaña, J.C., 2007b. What do the HIRM and S-ratio really measure in environmental magnetism? Geochem. Geophys. Geosyst. 8, Q09011. doi:10.1029/2007GC001717.
Liu, Q.S., Barrón, V., Torrent, J., Eeckhout, S., Deng, C.L., 2008. Magnetism of intermediate hydromaghemite in the transformation of 2-line ferrihydrite into hematite and its paleoenvironmental implications. J. Geophys. Res. 113, B01103. doi:10.1029/2007JB005207.
Lovley, D.R., Stolz, J.F., Nord, J.L., Phillips, E.J.P., 1987. Anaerobic production of magnetite by a dissimilatory iron-reducing microorganism. Nature 330, 252–254.
Maher, B.A., 1998. Magnetic properties of modern soils and Quaternary loessic paleosols: paleoclimatic implications. Paleogeogr. Palaeoclimat. Palaeoecol. 137, 25–54.
Maher, B.A., Taylor, R.M., 1988. Formation of ultrafine magnetite in soils. Nature 336, 368–370.
Maher, B.A., Thompson, R., Zhou, L.P., 1994. Spatial and temporal reconstructions of changes in the Asian palaeomonsoon—a new mineral magnetic approach. Earth Planet. Sci. Lett. 125, 461–471.
Maher, B.A., Alekseev, A., Alekseeva, T., 2002. Variation of soil magnetism across the Russian steppe: its significance for use of soil magnetism as a palaeorainfall proxy. Quat. Sci. Rev. 21, 1571–1576.
Mehra, O.P., Jackson, M.L., 1958. Iron oxide removal from soils and clays by a dithionite–citrate system buffered with sodium bicarbonate. Clays Clay Miner. 7, 317–327.
Michel, F.M., Barrón, V., Torrent, J., Morales, M.P., Serna, C.J., Boily, J.-F., Liu, Q.S., Ambrosini, A., Cismasu, A.C., Brown Jr., G.E., 2010. Ordered ferrimagnetic form of ferrihydrite reveals links among structure, composition, and magnetism. Proc. Natl Acad. Sci. USA 107, 2787–2792.
Moskowitz, B.M., Jackson, M.J., Kissel, C., 1998. Low-temperature magnetic behavior of titanomagnetites. Earth Planet. Sci. Lett. 157, 141–149.

Mullins, C.E., 1977. Magnetic susceptibility of the soil and its significance in soil science: a review. J. Soil Sci. 28, 223–246.
Mullins, C.E., Tite, M.S., 1973. Magnetic viscosity, quadrature susceptibility, and frequency dependence of susceptibility in single-domain assemblies of magnetite and maghemite. J. Geophys. Res. 78, 804–809.
Nie, J.S., Song, Y.G., King, J.W., Egli, R., 2009. Consistent grain size distribution of pedogenic maghemite of surface soils and Miocene loessic soils on the Chinese Loess Plateau. J. Quat. Sci. 25, 261–266.
Oches, E.A., Banerjee, S.K., 1996. Rock-magnetic proxies of climate change from loess–paleosol sediments of the Czech Republic. Stud. Geophys. Geod. 40, 287–300.
Oldfield, F., Maher, B.A., Donoghue, J., Pierce, J., 1985. Particle-size related, mineral magnetic source–sediment linkages in the Rhode River catchment, Maryland. USA. J. Geol. Soc. Lond. 142, 1035–1046.
Peters, C., Dekkers, M.J., 2003. Selected room temperature magnetic parameters as a function of mineralogy, concentration and grain size. Phys. Chem. Earth 28, 659–667.
Radhakrishnamurthy, C., Likhite, S.D., 1993. Frequency dependence of low-temperature susceptibility peak in some titanomagnetites. Phys. Earth Planet. Inter. 76, 131–135.
Simša, Z., Zounová, F., Krupička, S., 1985. Initial permeability of single-crystal magnetite and Mn-ferrite. Czech. J. Phys. B 35, 1271–1281.
Singer, M.J., Fine, P., Verosub, K.L., Chadwick, O.A., 1992. Time dependence of magnetic susceptibility of soil chronosequences on the California coast. Quat. Res. 37, 323–332.
Singer, M.J., Verosub, K.L., Fine, P., TenPas, J., 1996. A conceptual model for the enhancement of magnetic susceptibility in soils. Quat. Int. 34–36, 243–248.
Skumryev, V., Blythe, H.J., Cullen, J., Coey, J.M.D., 1999. AC susceptibility of a magnetite crystal. J. Magn. Magn. Mater. 196–197, 515–517.
Soil Survey Staff, 2006. Keys to Soil Taxonomy (10th edition). United States Department of Agriculture, Natural Resources Conservation Service, Washington (DC).
Stephenson, A., 1971. Single domain grain distributions I. A method for the determination of single domain grain distributions. Phys. Earth Planet. Inter. 4, 353–360.
Sun, W.W., Banerjee, S.K., Hunt, C.P., 1995. The role of maghemite in the enhancement of magnetic signal in the Chinese loess–paleosol sequence: an extensive rock magnetic study combined with citrate–bicarbonate–dithionite treatment. Earth Planet. Sci. Lett. 133, 493–505.
Torrent, J., 1975. Estudio de los suelos de las terrazas del Río Esla en el tramo comprendido entre Benavente y Ardón. Thesis, Universidad Politécnica, Madrid, Ph. D.
Torrent, J., 1976. Soil development in a sequence of river terraces in Northern Spain. Catena 3, 137–151.
Torrent, J., Schwertmann, U., Schulze, D.G., 1980. Iron oxide mineralogy of some soils of two river terrace sequences in Spain. Geoderma 25, 191–208.
Torrent, J., Barrón, V., Liu, Q.S., 2006. Magnetic enhancement is linked to and precedes hematite formation in aerobic soil. Geophys. Res. Lett. 33, L02401. doi:10.1029/2005GL024818.
Torrent, J., Liu, Q.S., Bloemendal, J., Barrón, V., 2007. Magnetic enhancement and iron oxides in the Upper Luochuan loess–paleosol sequence. Chinese Loess Plateau. Soil Sci. Soc. Am. J. 71, 1570–1578.
Torrent, J., Liu, Q.S., Barrón, V., 2010a. Magnetic minerals in Calcic Luvisols (Chromic) developed in a warm Mediterranean region of Spain: origin and paleoenvironmental significance. Geoderma 154, 465–472.
Torrent, J., Liu, Q.S., Barrón, V., 2010b. Magnetic susceptibility changes in relation to pedogenesis in a Xeralf chronosequence in northwestern Spain. Eur. J. Soil Sci. 61, 161–173.
Verosub, K.L., Fine, P., Singer, M.J., TenPas, J., 1993. Pedogenesis and paleoclimate: interpretation of the magnetic susceptibility record of Chinese loess–paleosol sequences. Geology 21, 1011–1014.
Vincent, K.R., Bull, W.B., Chadwick, O.A., 1994. Construction of a soil chronosequence using the thickness of pedogenic carbonate coatings. J. Geosci. Educ. 42, 316–324.
Walden, J., Oldfield, F., Smith, J., 1999. Environmental magnetism. A practical guide. Technical Guide No. 6., Quat. Res. Assoc., London.
Worm, H.-U., 1998. On the superparamagnetic-stable single domain transition for magnetite, and frequency dependency of susceptibility. Geophys. J. Int. 133, 201–206.
Zhou, L.P., Oldfield, F., Wintle, A.G., Robinson, S.G., Wang, J.T., 1990. Partly pedogenic origin of magnetic variations in Chinese loess. Nature 346, 737–739.